# Vortex-induced Morphology on a Two-fluid Interface and the Transitions

J.-C. Tsai[1,*], C.-Y. Tao[1], Y.-C. Sun[2], C.-Y. Lai[3,†], K.-H. Huang[3] , J.-R. Huang[2] and W.-T. Juan[1]

[1] *Institute of Physics, Academia Sinica, Taipei, Taiwan 11529*
[2] *Department of Physics, Nat'l Taiwan Normal University and*
[3] *Department of Physics, Nat'l Taiwan University*
(Dated: 2015.04.19+.RFI-2014vortex-jc20150428a.tex)

We investigate experimentally the steady flows in a cylinder containing two immiscible liquids, with the primary fluid being driven by the upper boundary rotating at constant speeds. The system exhibits interesting interplays between the flow fields and the morphology of the interface, with evidence showing that the remarkable flat-top structure is a consequence of the vortex breakdown discovered decades ago, and that the deformability of the interface also feedbacks positively to the development of the vortices. Monitoring the topological structure of the flow fields defines the base states and transitions behind the morphology, whereas our survey over different aspect ratios also reveals rich phenomena of surface instabilities accompanying these steady states.

The flow driven by a rotating disk at one end of a cylindrical container has become one of the classic problems in fluid mechanics [1–18]. In the case of a single Newtonian fluid, the flow can be fully characterized by the aspect ratio and a Reynolds number specified by the rotation rate, the radius, and the kinetic viscosity. The phenomena of vortex breakdown, namely the emergence of distinct loops in its secondary flow (velocity in the meridional plane), have been reported since the 1980s' [1, 2] with extensions to cases with an open surface [3, 4]. These vortex structures have sparked series of research works with simulations [5–8] and theories [9–11] and have also been utilized as an indicator of the viscoelastic properties of complex fluids, as reviewed extensively by Stokes et al. [12]. However, discussions on the consequences of these vortices beyond the velocity fields themselves seem still unseen in the literatures.

The use of two immiscible liquids in this classic setup introduces a highly deformable surface which, interestingly, serves as a sensitive indicator of the state of the flow: part of the morphology, with the most notable being the state of a plateau, has been reported by one of our authors with follow-ups [19–22] and also independently by Fujimoto and Takeda[23, 24] since 2009. In this work, we present evidence showing that such flap-top structure is a result of the long-discovered vortex, and that the deformability of the interface favors the development of the vortex. Our survey of the full parameter space also reveals instabilities such as liquid breakups and the breaking of the azimuthal symmetry, demanding extensions from existing knowledges in the research communities [25–32]. On the theoretical side, despite many existing simulations with either an open-surface [13–16] or a two-fluid interface [17, 18], the rich collection of morphologies and transitions have not yet been predicted, to the best of authors' knowledge.

Figure 1(a) shows the schematics of our experiments: inside the acrylic cylinder of radius 7.2 cm, we use soybean oil (manufactured by Uni-president Corp. in Taiwan) as the upper fluid and water as the lower one,
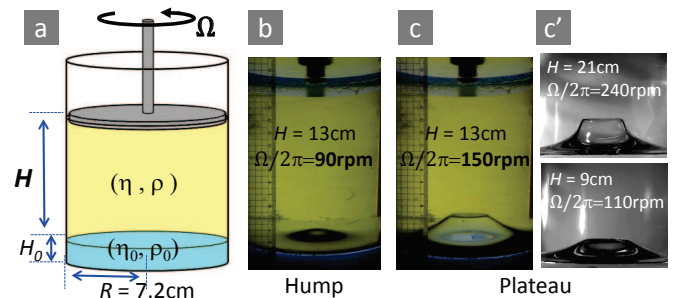


FIG. 1. Schematics of the setup and definition of parameters (a), back-lit photographs of the hump (b) versus the plateau at $H/R \approx 2$ with $H_0 = 1.5$ cm taken with a tilt angle (c), as well as the exact horizontal projections of the same state at $H/R \approx 3$ and $H/R \approx 1$ respectively (c'). The rotation rates are indicated in units of r.p.m.(revolution per minute).

giving a viscosity contrast $\eta/\eta_0 \approx 60$ and density ratio $\rho/\rho_0 \approx 0.92$. The flow is driven by the top boundary rotating at a constant angular speed $\Omega$, with a surrounding gap smaller than 1 mm such that the excess fluid above the disk, if any, would have little effect on the flow inside except for offsetting its pressure field. Photographs in Fig. 1(b-c) demonstrate the change of morphology from a simple hump at the low-speed limit, to the state of a plateau — a quite notable flat-top structure seen in a considerable range of aspect ratios and driving rates. We have also verified that the morphology reported here is generally insensitive to the change of the thickness of the lower fluid $H_0$ from 1 cm to nearly 1 meter [20], presumably because of the large viscosity contrast that makes the lower fluid almost entirely passive. Therefore the two main control parameters in our experiments are the height $H$ and the rotation rate $\Omega/2\pi$.

We investigate the flow of the upper fluid by video imaging the tracer particles seeded inside with false-colored post processing, detailed in endnote [33]. Figure 2 shows the development of the secondary flow along
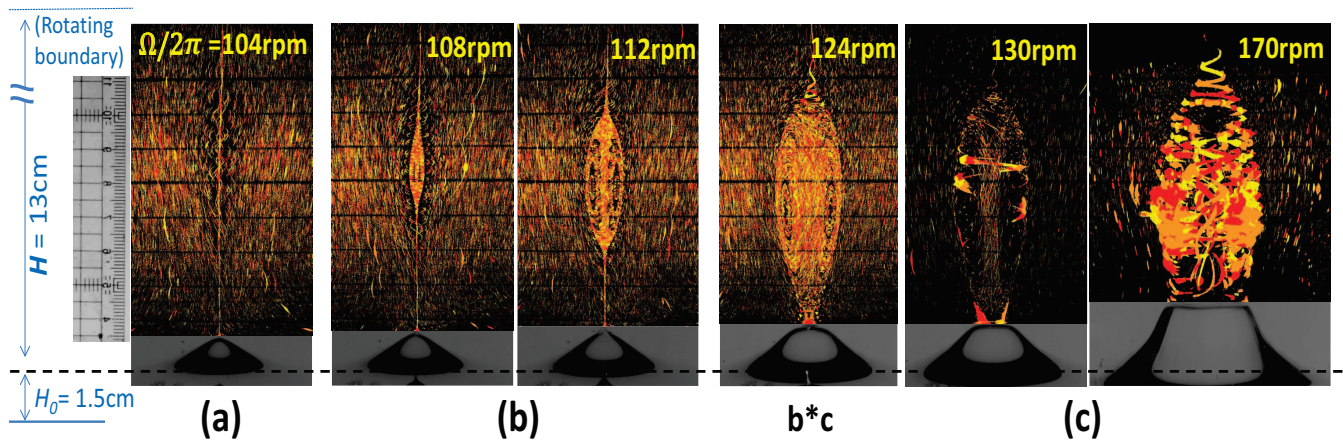
FIG. 2. Composite pictures to characterize the fluid flow above the hump (a, b) or the plateau (c), as the rotation rate $\Omega/2\pi$ increases. The pictures combine the use of slice illumination of fluid tracers (in false colors, detailed in endnote [33]) and back lighting of the interface below. The spacing between dark lines in the upper part of these pictures indicates the scale of 1 cm. Images in panel (c) are also interfered by droplets that are unintendedly generated during the transients, but the spatial structure of the flow is still recognizable.

with its interplay with the two-fluid interface, as it changes from a hump to a plateau upon the increase of rotation rate at a fixed aspect ratio $H/R \approx 2$. These post-processed pictures reveal not only the direction but also the magnitude of the flow. For instance, the image near the center of Fig. 2(a) indicates an upward flow at a speed about 1.6 cm/s, which reveals a significant slowdown from the asymptotic value $0.89\sqrt{\eta\Omega/\rho}$ for the axial flow in an idealized Karman pumping (without the confinement of the cylinder), which gives $\approx 2.5$ cm/s at $\Omega/2\pi =104$ r.p.m. Increasing the rotation rate results in the occurrence of a vortex and its growth in size (b), followed by the merge with the interface (b*c) and the further coupling between the vortex and the surface (c). Some of the images also shows spiraling trajectories near the central axis – see the upper part of b*c, for instance – as the result of our using a 5mm-thick illumination slice.

Close inspections of the tracer images allow us to identify transitions of topology defined by the separatrices in the secondary flow, providing a clear definition of the stage of change behind the morphology. The upper panels of Fig. 3 summarize the sequence of the slowdown of axial velocity (a), the emergence of a vortex and stagnation points (b), and most importantly, the descent of $S1-$ and its merge with the interface (b*c). Upon further increase of the rotation rate, part of the separatrices once connected to point $S1-$ would be detoured to connect the interface by a contour $C-$, that defines the edge of the plateau (c). Interestingly, at moderate aspect ratios, the top of the surface can maintain essentially flat for a considerable range of rotation rate (up to the onset of waves around the structure). The change into the flattop is reasonable because the flow in the upper fluid, as shown schematically by the graph, no longer provides

an upward forcing that could maintain a hump at lower rotation rates. The data graph shows our measurement of the height of the two stagnation points and the plateau width $W$, as functions of the rotation rate at $H/R \approx 2$.

The aspect ratio $H/R$ controls the total scenarios that are accessible by experiments. The lower panels of Fig. 4 show that, at a low aspect ratio, the scenarios can also include the merging of stagnation point $S1+$ with the interface (c*d), followed by the creation of an additional hump on top of the plateau (the state d, previously reported as a "double mound" in Ref. [19]). This can be understood as the consequence of a second transition, upon which the axial flow just above interface undergoes another switch of sign so that the forcing near the center of the plateau becomes upward again.

The role of the deformability of an interface on the vortex breakdown can be understood by comparing our experiment to a historical counterpart with a rotating disk below and an open surface above [3], in which the air plays the role of the lower fluid in our experiment except that the action of gravity is inverted and that the interface deformation is highly suppressed by the large density contrast. The historical experiment also had the primary liquid much more viscous than the other side of the interface, with the sequential development of the vortex being also qualitatively similar to ours. But quantitatively, at $H/R \approx 2$, the vortex did not become visible until its Reynolds number went beyond 1300, whereas in our experiment the vortex is already well developed as to reach the interface at the characteristic rotation rate $\Omega_{b*c}$ giving a Reynolds number $\Omega_{b*c}R^2/\nu \approx 900$. In fact, throughout our survey of the parameter space up to $H/R \approx 4$ (to be discussed with Fig. 4), signs of vortex interactions consistently occur at Reynolds numbers
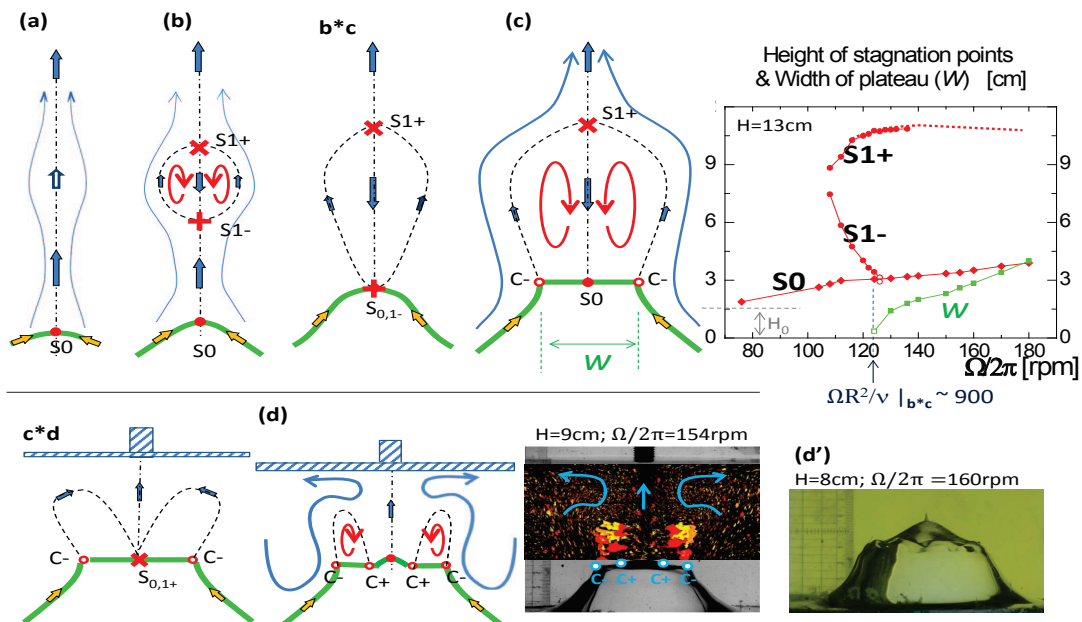
FIG. 3. Transitions of topology in the secondary flow. Arrows indicate the direction of the flow along the streamlines or the separatrices (represented by dashed lines), while stagnation points are labelled as $S1-$ and $S1+$. Panels (a) to (c) illustrate the emergence of the vortex and its relation with the interface, with our measurements of stagnation heights and the plateau width for $H=13$cm. At lower aspect ratios, the scenario is further extended to the emergence of an additional hump on top of the plateau with azimuthal symmetry (d) or with wavy patterns around the structure (d'). Note the successive merging of $S1-$ and $S1+$ with the interface, creating circular contours like $C-$ and $C+$ to which the separatrices are detoured.
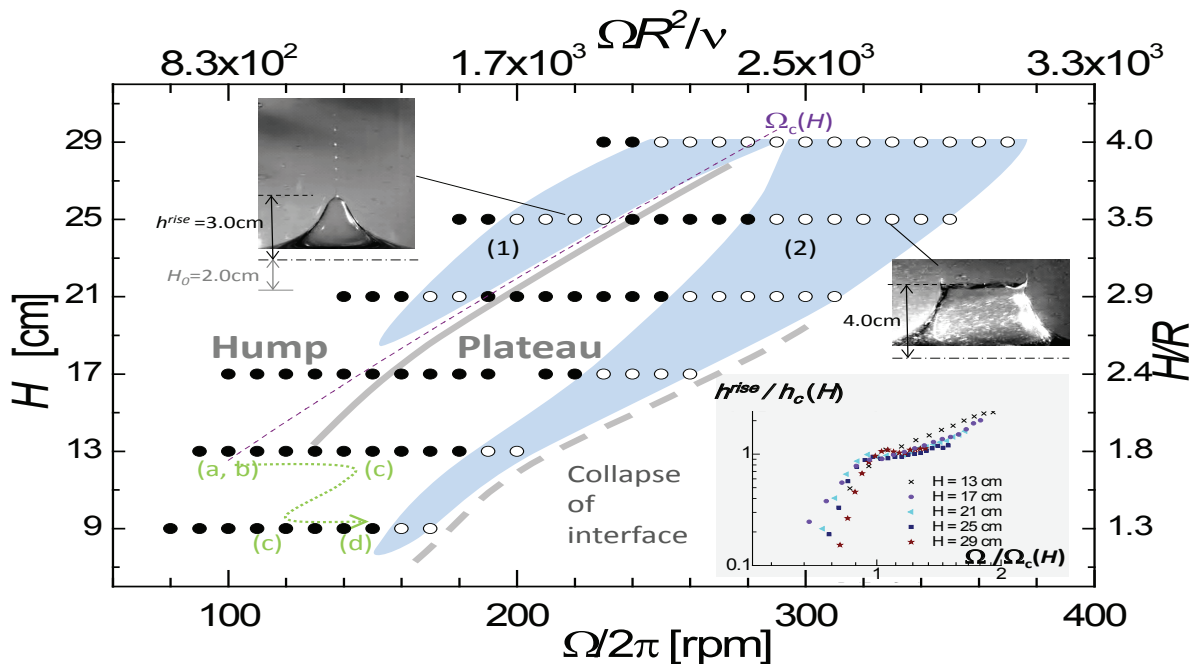


FIG. 4. Diagram summarizing the changes in morphology over various height $H$ and rotation rate $\Omega/2\pi$. The hump-plateau divide is marked by the gray line, while the boundary for the collapse of the interface by the thick dashed line on the right. The shaded Region (1) indicates the parameter space in which sustained breakup of liquid drops along the central axis is observed, whereas Region (2) indicates the occurrence of waves with breakups around the plateau. The inset graph summarizes the measured $h^{rise}$ versus $\Omega$ at various heights, revealing the common feature of a kink.

that are significantly lower than those threshold values reported in Ref. [3]. All evidence suggests that deformation of the two-fluid interface plays an important role that favors the development of vortices.

Figure 4 shows our survey of steady-state morphology and the transitions for a wide range of aspect ratio upto four, with the rotation rates indicated by the circles. The thick solid line represents the hump-plateau divide, while the thick dashed line on the right indicates the boundary beyond which the interface becomes unstable and collapses. The dotted curve with an arrow represents the route of transitions already described in Fig. 3(a-d). At a sufficiently high aspect ratio, we see one additional feature that the upward flow can become strong enough to overcome the surface tension and induce sustained ejections of the lower fluid along the center axis, marked as the shaded Region (1). They resemble the processes of viscous withdrawl and breakups that have been studied extensively in previous works [25–29]. However, further increase of the rotation rate does not enhance the ejections indefinitely: instead, the ejection subsides and eventually stops. Such transition of the interface implies that the upward stretching by the fluid flow has decreased so that the forcing can no longer exceed the surface tension. This can be regarded as another signature of vortex-interface interaction as they approach each other, preceding the creation of the flattop when one of the stagnation point does merge with the surface.

The total rise of the two-fluid boundary from its height at the rest state provides another indicator of the vortex-interface interactions. The inset graph in Fig. 4 shows our measurement of the $h^{rise}$ as functions of the rotation rate, revealing a common feature of a kink at a characteristic rotation rate $\Omega_c$ and $h_c$ for each $H$. These characteristic values are determined by the best fit to observed kinks with a smooth function of $H$, as explained in endnote [35]. Note the trends that (1) the values of $\Omega_c(H)$, represented by a thin dashed line on the main graph, is close to the onset of the vortex at a low aspect ratio but becomes nearly indistinguishable from the hump-plateau divide as $H$ increases, and that (2) the kink in $h^{rise}$ versus $\Omega$ becomes sharper at higher values of $H$. These two facts can be consistently explained by the picture that, at low aspect ratios, the interface is already strongly affected by the vortex upon its first occurrence whereas, at high aspect ratios, the emergence of a vortex happens relatively far away from the interface therefore its "hindrance" [20] on the rising of the interface is not effective until their close encounter, therefore the change in the slope of $h^{rise}(\Omega)$ appears relatively abrupt.

In addition, the shaded Region (2) in Fig. 4 indicates the parameter space where we observe wavy patterns around either the flattop (state c) or a double mound (state d). The patterns break the azimuthal symmetry and are often accompanied by the breakup of liquid drops, in many cases also preceding the catastrophic

collapse of the interface. In practice, the wavy patterns could also prevent us from defining the width of the flat-top. The exact mechanism for the symmetry breaking leading to these patterns demands further investigations, while it is believed that a slight asymmetry in the driving can trigger the instability [30, 31]. At an aspect ratio as high as $H/R \approx 4$, we find that the such instabilities occurs almost at the hump-plateau divide: the merging of Region (2) with Region (1) marks the practical limit for precise characterizations of the plateau, although the waviness accompanied by the outward ejection of liquid drops still provides the visual evidence of a vortex interacting with the interface. High-speed videos and further information regarding the two types of surface instabilities are available online [33].

In summary, the use of a two-fluid interface with a fractional density difference allows us to revisit the classic vortex breakdown problems and to identify several interesting consequences. It is the long-discovered vortex that shapes the flat-top structure, while the deformability of the interface also feedbacks positively to the development of the vortices. The changes of morphology of the interface are connected to the underlying transitions of topology defined by the separatrices in the velocity fields. We also present a full diagram of steady-state morphology that, on one hand, illustrates the interplays between a deformable surface and the classic vortices while, on the other hand, exhibits unexplored phenomena involving liquid breakups and symmetry breaking and offers fruitful test grounds for theories on these instabilities.

———

* Correspondence: JC Tsai<jctsai@phys.sinica.edu.tw>
† Currently in Princeton University, NJ.

[1] M. Escudier, Expt. Fluids **2**, 189 (1984).
[2] A. Prasad and R. Adrian, Expt. Fluids **15**, 49 (1993).
[3] A. Spohn, M. Mory, and E. Hopfinger, Expt. Fluids **14**, 70 (1993).
[4] A. Spohn, M. Mory, and E. Hopfinger, J. Fluid Mech. **370**, 73 (1998).
[5] H. J. Lugt and M. Abboud, J. Fluid Mech. **179**, 179 (1987).
[6] J. M. Lopez, J. Fluid Mech. **221**, 533 (1990).
[7] G. L. Brown and J. M. Lopez, J. Fluid Mech. **221**, 553 (1990).
[8] J. P. Watson and G. P. Neitzel, Phys. Fluids **8**, 3063 (1996).
[9] J. J. Keller, Phys. Fluids **7**, 1695 (1995).
[10] S. A. Berger and G. Erlebacher, Phys. Fluids **7**, 972 (1995).
[11] Z. Rusak, J. Fluid Mech. **323**, 79 (1996).
[12] J. R. Stokes, L. J. W. Graham, N. J. Lawson, and D. V. Boger, J. Fluid Mech. **429**, 67 (2001).
[13] J. M. Lopez, F. Marques, A. H. Hirsa, and R. Miraghaie, J. Fluid Mech. **502**, 99 (2004).

[14] D. Lo Jacono, M. Nazarinia, and M. Brøns, Phys. Fluids **21**, 111704 (2009).

[15] R. Bouffanais and D. Lo Jacono, Phys. Fluids **21**, 064107 (2009).

[16] L. Kahouadji and L. M. Witkowski, Phys. Fluids **26**, 072105 (2014).

[17] P. T. Brady, M. Herrmann, and J. M. Lopez, Phys. Rev. E **85**, 016308 (2012).

[18] M. A. Herrada, V. N. Shtern, and J. M. López-Herrera, Phys. Fluids **25**, 093604 (2013).

[19] C.-Y. Lai and T.-A. Ku, in *Intel International Science and Engineering Fair* (Reno, Nevada, 2009).

[20] Presentation at the *64th Annual Meeting of the Division of Fluid Dynamics, American Physical Society (APS-DFD)*, Baltimore, Maryland, 2011, http://meetings.aps.org/link/BAPS.2011.DFD.R19.2

[21] Presentation, *65th APS-DFD*, San Diego, California, http://meetings.aps.org/link/BAPS.2012.DFD.A28.2

[22] Presentation, *67th APS-DFD*, San Francisco, California, http://meetings.aps.org/link/BAPS.2014.DFD.A11.3

[23] S. Fujimoto and Y. Takeda, Phys. Rev. E **80**, 015304 (2009).

[24] S. Fujimoto, Y. Murai, Y. Tasaka, and Y. Takeda, J. Visualization **13**, 17 (2010).

[25] I. Cohen and S. R. Nagel, Phys. Rev. Lett. **88**, 074501 (2002).

[26] I. Cohen, Phys. Rev. E **70**, 026302 (2004).

[27] S. C. Case and S. R. Nagel, Phys. Rev. Lett. **98**, 114501 (2007).

[28] M. K. Berkenbusch, I. Cohen, and W. W. Zhang, J. Fluid Mech. **613**, 171 (2008).

[29] F. Blanchette and W. W. Zhang, Phys. Rev. Lett. **102**, 144501 (2009).

[30] T. R. N. Jansson, M. P. Haspang, K. H. Jensen, P. Hersen, and T. Bohr, Phys. Rev. Lett. **96**, 174502 (2006).

[31] B. Bach, E. C. Linnartz, M. H. Vested, A. Andersen, and T. Bohr, J. Fluid Mech. **759**, 386 (2014).

[32] T. Suzuki, M. Iima, and Y. Hayase, Phys. Fluids **18**, 101701 (2006).

[33] The upper fluid, with a small amount of high-reflection neutral-bouyant glass spheres as tracers, is illuminated by a vertical slice of laser aligning with the central axis. The side-view images are captured through an additional liquid-filled square tank surrounding the cylinder to correct the distortion. Pictures are generated by superposing hundreds of consecutive video frames (typically at 10 frame/s), with a cycle of three colors (red, orange, then yellow) to distinguish intervals of every 1s. Full-resolution pictures are available online through http://www.phys.sinica.edu.tw/jctsai/vortex/ , along with video clips demonstrating instabilities on the interface.

[34] G. Batchelor, *An Introduction to Fluid Dynamics*, (Cambridge University Press, 2000), Section 5.5

[35] The characteristic values $h_c(H)$ and $\Omega_c(H)$ are defined by the empirical power-low relations with $H/R$ based on the best fits to the kinks observed in our experiments: $h_c/R = 0.048(H/R)^{1.55}$ and $\Omega_c R^2/\nu = 418(H/R)^{1.24}$ with $\nu = 0.52$ cm$^2$/s.